EFDA–JET–PR(08)17

M.Goniche, A.Ekedahl, J.Mailloux, V.Petržílka, K.Rantamäki, P.Belo,
G.Corrigan, L.Delpech, K.Erents, P.Jacquet, K.Kirov, M.-L.Mayoral,
J.Ongena, C.Portafaix, M.Stamp, K.-D.Zastrow
and JET EFDA contributors

SOL Characterisation and LH coupling Measurements on JET in ITER-Relevant Conditions

SOL Characterisation and LH Coupling Measurements on JET in ITER-Relevant Conditions

M.Goniche[1], A.Ekedahl[1], J.Mailloux[2], V.Petržílka[3], K.Rantamäki[4], P.Belo[5], G.Corrigan[2], L.Delpech[1], K.Erents[2], P.Jacquet[2], K.Kirov[2], M.-L.Mayoral[2], J.Ongena[6], C.Portafaix[1], M.Stamp[2], K.-D.Zastrow[1] and JET EFDA contributors*

JET-EFDA, Culham Science Centre, OX14 3DB, Abingdon, UK

[1]CEA, IRFM, F-13108 Saint Paul-lez-Durance, France
[2]Association EURATOM-UKAEA, Culham Science Centre, Abingdon, OXON OX14 3DB, UK
[3]Association IPP.CR, 182 21 Praha 8, Czech Republic
[4]Association EURATOM-Tekes, VTT, P.O.Box 1000, FI-02044 VTT, Finland
[5] Associação Euratom-IST, Centro de Fusão Nuclear, 1049-001 Lisboa, Portugal
[6]Plasmaphysics Lab, ERM-KMS, Association EURATOM-Belgian State, Brussels,
** See appendix of M.L.Watkins et al., Fusion Energy 2006 (Proc. 21st Int. Conf. Chengdu, 2006) IAEA, (2006)*

Preprint of Paper to be submitted for publication in Nuclear Fusion

ABSTRACT

Lower Hybrid (LH) Current Drive experiments have been carried out on JET with a gap varying between 0.09 and 0.16m, and LH power in the range of 0-3.2MW. For different plasma configurations, the electron density n_e of the scrape-off layer has been studied by the mean of a reciprocating Langmuir probe magnetically connected to the LH antenna. For pulses in the high confinement regime (H mode) characterized by strong particle bursts in the plasma edge, the Edge Localized Modes (ELMs), profiles of the saturation current (J_{sat}) are obtained with a sufficient time resolution to distinguish 'between ELMs' and during the rise and decay of the ELMs.

It is found that gas injection from a valve located near the LH launcher and magnetically connected to it allows to rise the density and improve the LH coupling. The J_{sat} profiles indicate quite clearly that this density rise affects mainly the plasma layer in front of the antenna with a typical thickness of 5cm. The resulting profile can be extremely flat in this region. The effect of the near-launcher gas injection but also of the LH power and the total gas injection on the density at the wall is quantitatively documented. It is shown in particular that with increasing LH power, the required gas injection for obtaining good LH coupling is decreasing, with no saturation obtained so far. Effect of the ELMs on the LH coupling is also discussed. Modelling with the EDGE2D code indicates that such flat profiles of J_{sat}/n_e can be obtained when LH power dissipation is taken into account. Detailed analysis of the heat flux carried by electrons accelerated in the near-field of the antenna confirms the increase of density with gas puff during high LH power coupling.

1. INTRODUCTION

Lower Hybrid (LH) waves have proved to be very powerful for shaping the plasma current profile thanks to its current drive (CD) capability in a hot plasma. LH current drive has been extensively used on JET [1,2] and on JT60-U [3] to obtain reversed magnetic shear plasmas with the minimum value of the safety factor q_{min} exceeding 2. This configuration leads to an enhanced confinement in the plasma core resulting from the onset of an Internal Transport Barrier located at a normalized radius ϱ which may be as large as $\varrho = 0.6$ [3]. Such a scenario is envisaged for ITER, with a power amplification factor Q~5 and a burn time of 3000s.

The coupling of the slow wave to the plasma is a critical issue which is still difficult to extrapolate from present tokamaks to the next generation. For ITER, scrape-off layer (SOL) modelling with the B2-EIRENE code stops 4cm behind the separatrix [4] whereas the distance D_{sa} between the separatrix and the antenna face will be as large as $D_{sa} = 0.15 - 0.20$m. Moreover in ITER the plasma position control will have a large time constant which could lead to slow adaptations of the plasma position in front of the launcher. Methods which render LH coupling rather insensitive to the exact position of the plasma separatrix are therefore a necessity. In most of the experiments, antennas operate with a 'gap' (i.e. separatrix-antenna distance) of $D_{sa} = 0.03 - 0.06$m. Early experiments on ASDEX in L-Mode allowed to couple high power density (~12MW/m^2), with Dsa as large as 0.09m. This was even improved to D_{sa}=0.11m with gas puffing from a valve close to the launcher [5]. Increase

of electron density near the launcher was inferred from reflectometry measurements. On JT-60U, favourable effects of puffing gas near the launcher was observed and good LH coupling with D_{sa} =0.155m was reported with a multijunction-type antenna but this experiment was performed at a moderate power density (<10MW/m^2) [6]. Note that in these experiments the LH antenna was 5mm behind the first wall, in a region where the density decay length is rather small, rendering good coupling more challenging. On the same machine during ELMy H-mode plasmas, reasonably low power reflection coefficients (RC) are measured with a gap up to 0.13m when recycling conditions are favourable [3]. Similar results of coupling with a large gap were found on Tore Supra in limiter configuration [7]. In this case, the Last Closed Flux Surface (LCFS) position is fixed and the LH power is slowly ramped-up (~1s). Langmuir probes embedded in the LH launcher indicate clearly that the density rises quasi-linearly with LH power and a large power density (24MW/m^2) was successfully coupled with an average RC of 5% and Dsa varying between 0.09 and 0.12m. From a data base with Dsa varying between 0.04m and 0.14m, the beneficial effect of enhanced recycling on LH coupling at large D_{sa} in this limiter machine was assessed [8].

On JET, early experiments demonstrated that the distance from the LH launcher to the LCFS could be significantly increased by injecting gas from the Gas Introduction Module 6 (GIM6), a poloidally extended source ~1.2m toroidally far away from the launcher and magnetically connected to it. In this configuration ~2MW (8MW/m^2) was coupled in LH-only heated plasma (L-mode) with D_{sa} =0.09m for the lower rows of waveguides of the antenna and D_{sa} =0.06m for the upper rows. The non-linear response of the electron density in front of the LH launcher to the gas rate leads to an hysteresis cycle and the maximum distance for which good coupling (RC<5%) is obtained with no injection from GIM6 is increased by ~2cm after strong gas injection [9]. During these experiments, no edge density measurements were available and the combined effect of neutrals provided by the intrinsic (recycling) or extrinsic (gas valve) source with the ionization provided by the LH wave could be just inferred from the RC coefficient measurements. This can lead to misinterpretation: the RC is not an univocal function of the density and non-linear effects may occur at high LH power density.

During the JET 2003 campaigns, high power LHCD experiments (with up to 3MW of LH power) have been carried out with a gap D_{sa} varying between 0.07 and 0.11m in ELMy H-mode plasmas [10, 11]. Both methane (CD_4) and deuterium (D_2) were used to raise the density in the SOL. From reciprocating probe (RCP) measurements, D2 was found to be more efficient than CD_4. More recently, LH coupling has been investigated for pulses performed with a gap varying between 0.10m and 0.16m in different plasma configurations. In all these shots the RCP was used for SOL measurements. Deuterium was injected from GIM6 at various rates. Combined with the 2003 shots, a database of 60 time slices including RCP and LH coupling measurements has been established. In this paper, we report on these measurements and will focus on the consistency of the density measurements with the RC measurements. The effect of ELMs is also documented. The crucial question on the mechanism driving this increase of density (increase of the source by enhanced ionization and/

or increase of the transport) will be addressed with EDGE2D-NIMBUS simulations. Finally, the analysis of the heat flux deposition on a plasma facing component magnetically connected to the LH antenna provides additional information on the electron density variation with increasing LH power in the near-field of the antenna.

2. EXPERIMENTAL SET-UP

The LH launcher, composed of 12 rows of 36 waveguides (including two passive waveguides at each side for mitigation of the edge effects), has already been described in ref. [12,13]. Four adjacent waveguides (the multijunction) of the same row and two multijunctions of adjacent rows are fed by the same RF input. Consequently the RF measurements consists of an array of 6 rows (labelled 1 to 6 from top to bottom) by 8 columns. For the reported experiments, it should be stressed that not all the klystrons were pulsing and only between ~60% and 83% of the antenna was powered. Due to the strong cross-coupling of the waveguides via the plasma, this may lead to an increase of the power reflection coefficients (RC) with respect of the ideal case. Note that in this paper we have recalculated the mean RC for each row in the JET database, in order to leave out those modules with technical difficulties or drifts in the calibrations. The launcher is positioned 20mm (instead of 5mm for the 2003 experiments behind the poloidal limiters (PL). However the limiter located on the electron drift side of the launcher is 5mm behind the other PLs and the field lines passing in front of the launcher have a connection length L//~2.5 m in the shadow of the two PLs neighbouring the launcher. As a reference to the new results discussed in this paper, we used the data from LH coupling studies at JET done in 2003. In those experiments, the launcher was positioned 5mm behind the poloidal limiters, and the launcher was aligned with the retracted limiter leading to L//~4.5m. During LH power injection, GIM6 (whose arrangement is detailed in [10]) was systematically used aiming at raising the electron density in the flux tubes connected to the antenna or passing in front of the antenna.

The RCP, located in an upper port of the machine, provides measurements from the far SOL up to a distance behind the separatrix varying between 0.03 and 0.07m. The radial coordinate of the magnetic surface, connected to the probe, in the equatorial plane (labelled R) is derived from the equilibrium EFIT code. For the range of q_{95} of these experiments, the field line connected to the RCP can either be passing slightly below the LH launcher or being connected to the lower rows (4 to 6) of the launcher (figure 1). The field lines behind the PLs connected to the RCP are connected on the electron drift side by carbon tiles protecting the upper part of the vessel. This leads to a connection length varying between L//~4m and L//~6m depending on the exact q95 value. It is therefore expected a slightly shorter decay length in front of the LH launcher (when retracted by 20mm) than that measured by the RCP.

The bias voltage of the RCP is swept from –200V to +50V in 5ms with a data acquisition rate of 20kHz. The sweep frequency (200Hz) is often too low with respect to the ELM frequency (20-200Hz) and the electron density (n_e) and temperature (T_e) data are frequently spoiled by the ELMs.

In order to get a reliable variable for all shots, the saturation current J_{sat} between ELMs is used. This signal is obtained by discarding the current data when the Dα signal exceeds by more than 30% the baseline and when the voltage exceeds –150V. At a distance from the separatrix larger than 0.03m, T_e is below 40eV and J_{sat} is correctly estimated by this procedure. A J_{sat} profile as a function of the distance to the separatrix $R-R_{sep}$ is shown on figure 2. The ~35 samples obtained at almost constant radius ($\Delta R<1$mm) can be averaged to smooth the effect of the fluctuations and the residual variation of density between the ELMs. Three regions can be seen: the 'close' SOL ($R-R_{sep}<0.06$m) where the signal decreases exponentially with an e-folding decay length $\lambda J\sim0.02$m, the 'far' SOL ($0.06<R-R_{sep}<0.10$m) where the density levels off and the SOL ($R-R_{sep}>0.10$m) in the shadow of the limiters where J_{sat} decreases sharply. The flatness of the far SOL can vary from one shot to another and will be discussed later. Note that the density profile in the LH private zone (i.e. between the PL neighbouring the LH antenna) has a short connection length and cannot be measured. Consequently we will quote Jsat at R=RPL and label this quantity J_{sat}@wall. Assuming an electron temperature Te=20eV, $T_e=T_i$ and no flow (Mach number M=0), J_{sat}@wall =104A/m^2 indicates an electron density ne=4×10^{18}m^{-3}. Flows have been measured in the JET SOL and M~0.3 have been measured 60mm behind the separatrix [14]. This would lead to an overestimation of n_e by 10%. Further overestimations could result when the ion temperature is larger than electron temperature. For the analysis of the results, the $T_e^{1/2}$ contribution for j_{sat} will be neglected and a j_{sat} evolution will be interpreted as resulting from a variation in n_e.

LHCD experiments have been carried out with a gap varying between 0.09 and 0.16m and LH powers up to 3.2MW. Two plasma shapes have been tested: (i) with low ($\delta_{up}/\delta_{low}=0.16/0.27$) and (ii) with high ($\delta_{up}/\delta_{low}=0.38/0.50$) triangularity. Plasmas were mainly heated by neutral beams, with input power ranging from 8 to 18MW. The LH power was applied during the H-mode phase with ELM frequencies varying between ~20Hz and ~200Hz. The plasma current (I_p=1.5-1.9MA) and toroidal field (B0=3-3.1T) were adjusted to meet the requirements of the advanced scenarios ($q_{95}\sim5$). For this configuration, the RCP is magnetically connected to the flux tubes passing in front of the LH antenna. Gas flows up to 9×10^{21}el./s from GIM6 have been applied during the LH phase. In some cases, GIMs distributed all around the divertor (GIM 9 and 10) were used.

A database of 70 time slices including RCP and LH coupling measurements has been established. For the analysis, two category of shots can be distinguished: shots performed with low triangularity δ and D_{sa} varying between 0.09 and 0.12m and those performed with high triangularity and D_{sa} varying between 0.14 and 0.16m. The quoted separatrix-antenna distance D_{sa} is measured in the equatorial plane. Due to the mismatch of the poloidal curvature of the launcher and the magnetic surfaces, this actual distance is shorter for the upper row (row 1) and larger for the lower row (row6). For the low δ configuration, the gap along the launcher is $D_{sa}\pm0.01$m. For the high δ configuration, the gap along the launcher is varying from $D_{sa}+0.01$m to $D_{sa}-0.015$m.

3. RCP MEASUREMENTS

When the LH power is increased the density rises in a layer which extends in front of the PL by several centimetres and a plateau is formed when the LH power is sufficiently high. This is illustrated in figure 3. By increasing the LH power from 0.4MW to 1.6MW with constant gas injection from GIM6 (fig.3a), the close SOL is marginally affected whereas a significant increase of Jsat is measured for $0.07<R-R_{sep}<0.10$m. Similar flat density profiles on front of the PL are obtained with a larger gap and a plasma with high δ (fig.3b). In that case the J_{sat} plateau extends from $R-R_{sep}=0.08$m to $R-R_{sep}=0.13$m.

The low power pulse of figure 3.b was performed with no gas injection (open circles) and beneficial effect of GIM6 is clear when the J_{sat} profile is compared to those with gas injection (closed symbols). The effect of LH power is different for the two scenarios. At high gap/high δ (fig.3b), J_{sat} in front of the PL has almost the same value ($\sim 1.2\times10^{4}$A/m^2) for PLH=0 (closed circles) and $P_{LH}=3.2$MW (closed squares) with relatively large gas injection ($F_{GIM6}=2\text{-}4\times10^{21}$el./s). For the low triangularity plasmas, EFIT equilibrium indicates that the field lines with $R-R_{sep}\geq0.06$m hit the top inner wall tiles at a poloidal angle $\theta \sim 120°$ (where $\theta=0$ is the equatorial plane on the low field side). Enhanced recycling (and carbon release as inferred from the strong increase of the CIII line intensity) with LH power could result from fast electrons accelerated in front of the launcher and intercepted by the wall [15]. The high δ configuration is close to a double-null configuration and the field lines intersect the wall at the very top of the vessel ($\theta\sim90°$) for $R-R_{sep}\geq0.02$m. In this case, the profiles from figure 3b suggest that ionisation induced by the wave is weak.

Such a plateau, with an e – folding decay length larger than 0.1m, is obtained experimentally in most of the cases when the applied LH power is sufficiently large. The exact role of gas injection is difficult to identify since there is an inter-play between the density in the SOL and the LH coupling: high power coupling requires sufficiently high density and the density is raised by the presence of LH waves. In order to clarify the respective role of gas injection and LH power, the current density on the magnetic surface grazing the leading edge of the poloidal limiters (labelled J_{sat}@wall) is plotted as a function of the LH power (fig.4a) and FGIM6 (Fig.4b) for $R-R_{sep}=0.10$m and low triangularity plasmas.

The beneficial effect of the LH power for increasing the density in front of the PL (the 'wall') is clearly seen from figure 4a. When the LH power is varied between 0 and 3MW, J_{sat}@wall increases by a factor ~6 with no indication of saturation. With the same data, when J_{sat} is plotted as a function of gas flux (figure 4b), one obtains a wider scattering of the points at high gas puffing values. Note that, as we will show later in the paper, an optimal value for J_{sat}@wall is $\sim 1.5\times10^{4}$A/m^2, implying from these figures, that moderate gas injection is required at high LH power. The same analysis is performed with the second series of shots performed with $R-R_{sep}=0.13$m and high δ. These high δ plasmas are characterized by higher recycling: for similar gas injection ($\sim4\times10^{21}$el./s), recycling estimated from the D_α line, viewing the equatorial plane on the low field side, increases by a factor ~1.8 as compared to low δ plasmas. In that case for both plots, we obtain a larger scattering of

the data (figure 5). In particular, it is found in some cases that high J_{sat}@wall (> 10^4A/m^2) can be obtained with gas injection (F_{GIM6}=4×10^{21}el./s) and no LH power. The density at the wall can be significantly increased by strong gas puffing from the modules distributed along the divertor ($F_{GIM9-10}$=1×10^{22}el./s). In that case, the central line-averaged density increases by ~10% and J_{sat}@wall from 1.1A/cm^2 to 1.9A/cm^2 for shots with PLH =2.3-2.4MW and F_{GIM6}=4×10^{21}el./s (arrows in figures 5a and b). The efficiency of LH power to raise the density, estimated from the slope of the plot of J_{sat}@wall as a function of PLH, is lower by a factor ~2 for the large gap and high δ series.

4. LH COUPLING MEASUREMENTS

LH coupling is measured from the RCs averaged for each of the 6 rows of modules (each containing two rows of waveguides). For the pulses of figure 5, the RC of row 2 (second upper row of the LH launcher) and row 6 (bottom row of the LH launcher) are plotted as a function of J_{sat}@wall in figure 6.

For J_{sat}@wall <1A/cm^2, the coupling is very weak and RC exceeds 20%, indicating that the density in front of the antenna is below the cut-off (ncut-off~1.7×10^{17}m^{-3}). The measured electron temperature at the PL radius is about 15eV, so the density, corresponding to J_{sat}@wall =1A/cm^2, is ne = 4×10^{18}m^{-3} (assuming no flow in the SOL). We conclude that the density falls off by one order of magnitude in the shadow of the PL for the 2006 shots with the launcher located 20mm behind the PLs. This is consistent with an e-folding density decay length λn~10mm. Optimal coupling conditions are obtained for J_{sat}@wall =1-2×10^4A/m^2. For higher values, RC slightly increases. According to coupling code predictions [16], this indicates that the density at the plasma-antenna interface exceeds ~10 times the cut-off density, provided that non-linear effects do not affect the coupling significantly. This fast transition is possible if we assume that the Jsat plateau measured in front of the PL actually extends from the antenna (0.02m behind the PL) up to a layer located ~0.05m in front of the PL. This transition is more pronounced for the lower rows (5 and 6), although these rows are more recessed from the plasma, suggesting that the density is larger at the bottom than at the top. It should be noted that the 2003 pulses (open symbols) were achieved with a smaller distance between the PL and antenna (5mm) and higher RC (~5%) in the high edge density regime, suggesting an even larger density for these pulses compared to the experiments from 2006. We found the same threshold of ~1×10^4 A/m^2 for the plasmas with high triangularity and a gap of 0.13m (figure 7). The fast transition short/long density decay length is clear from this figure: for the same measured J_{sat}@wall =1.1 A/cm^2, in one case poor coupling with a RC~10% is obtained and in another case good coupling with a RC~2%. The scenarios are quite different for these two pulses. In the first case, no gas from GIM6 was used but a large amount of gas was injected from GIM9-10 ($F_{GIM9-10}$=2×10^{22}el./s). In the second case, gas was only injected from GIM6 (F_{GIM5}=4×10^{21}el./s) and a strong effect of gas injection from this GIM on LH coupling is observed for the lower rows (row 5 and 6) but a weaker effect on the other rows.

The beneficial effect of heavy gas puff from GIM9/10 on all rows, but not on row 6, is also

illustrated on figure 8. In that case, the RC of the five upper rows are below 5-6% and the addition of $F_{GIM6}=4\times10^{21}$el./s (while the total gas flow is reduced) strongly reduces the RC of the last row below 2%. Comparing pulses with injection from GIM9-10 only (#67882) or GIM6 only (#67884), it is concluded that the same coupling on rows 1-5 is obtained with ~5 times less gas when injected from the connected gas module.

5. RCP AND LH MEASUREMENTS DURING ELMS

Edge Localized Modes (ELMs) are responsible for the loss of particles and energy in the plasma edge on a very short time scale, typically 200μs on JET [17],[18]. This leads to a transient increase of the density in the SOL. At first order the density amplification factor can be estimated from the ratio between the density at the top and the bottom of the pedestal which can exceed a factor ten. The fast acquisition of the RCP gives evidence that the particle flux (J_{sat}) measured at the LCFS can be increased by almost two orders of magnitude as shown on figure 9. For the high δ/large gap case, the effect of the ELMs seems weaker compare to low δ case but still important and the particle flux increases by a factor 3-4, 0.13m behind the separatrix and almost the same factor 2cm behind the poloidal limiters (figure 10). It should be noted that the relative increase of the density during an ELM should not be smaller in the shadow of the plasma facing components than in front of these components as we expect the e-fold decay length to be at least conserved.

During an ELM the RCs generally vary indicating clearly that the density in front of the launcher is modulated by this plasma edge perturbation. However for the whole database we did not find any case where a loss of power occurs due to the fast change of coupling. This result is consistent with coupling modelling indicating that the RC of a multijunction is a weak function of the density between $n_e\sim4\times10^{17}m^{-3}$ and $n_e\sim2\times10^{18}m^{-3}$and is expected to increase slowly when the density exceeds this upper limit such that high values for the reflected power which could exceed the threshold of the safety system are unlikely.

For the low recycling case, the beneficial effect of the ELMs on coupling is clearly identified when no gas is injected from GIM6: good coupling with RC<5% is achieved when the D_α signal is at least twice the base level (figure 11, pulse 66976, red and blue symbols). We only show the data for row 2 and row 6 as the data for row 1 and row 5, respectively, show essentially the same behaviour. They have also the same threshold for the low RC regime indicating that the density increase is homogeneous across the LH launcher front end. For the high recycling regime, very low RC are obtained for the upper row during the entire time sequence indicating that the density in front of the antenna is further increased with respect to the low recycling case, consistent with the D_α signal (Figure 11, pulse 67882, green and magenta symbols). The high recycling does not benefit to the lower row and poor coupling is obtained most of the time between the ELMs although RC below 10% is achieved during the ELMs.

For the two same plasma discharges, low RC is now obtained between ELMs and during ELMs (RC<5%) when gas is injected from GIM6 ($F_{GIM6}=4\times10^{21}$el./s). For the low recycling case, an

optimal density is reached for the lower row for medium amplitude of the ELMs (D_α~0.25) whereas the RC is continuously decreasing with the ELM amplitude for the upper row (figure 12, red and blue symbols). For large ELM perturbations (Dα>0.25), the experimental increase of the RC would suggest an increase of the density above ne~$3\times10^{18}m^{-3}$. For another discharge performed with higher gas rate ($F_{GIM6} = 5.7\times10^{21}$el./s), an optimal density is also found for the upper row. This occurs for an ELM amplitude larger than for the lower row. This suggests that during an ELM with gas injection the density is higher in front of the lower part of the antenna.

For the high recycling case, the RC of the upper row decreases with increasing ELM amplitude reaching very low values (<0.5%) for the largest ELMs (figure 12, green symbols). These low RC values are reached at large ELMs independent of the gas puffing. For the lower row, the RC increases for D_α>1 in a markedly different way than for the low recycling case (figure 12, magenta symbols).

It should be noted that in both configurations (low and high recycling), the coupling is identical for both rows when the D_α signal is minimum (corresponding roughly to the majority of the data between ELMs) and diverge during the ELMs. As expected, the base RCs between ELMs is lower for the high recycling case (~1%) than for the low recycling case (~4%).

Assuming that D_α is roughly proportional to the density in front of the launcher, we find the expected dependence of the RC with the density for the upper row and also for the lower row, in the case of low δ and no gas injection, but this is much less clear for the data from the lower row in all other cases. For the upper row, this would allow to estimate the density in front of the waveguides. With no gas injected from GIM6, the density in front of the launcher is close to the cut-off (n_e~$1.7\times10^{17}m^{3}$) between ELMs and increases to a density which can exceed n_e ~$10\times n_{cut\text{-}off}$ during the ELM for the low recycling case. For the high recycling case, although the gap between the LCFS and the antenna is 0.02m larger, the density is at least n_e~$3\times n_{cut\text{-}off}$ between ELMs and should at least double during the ELM bursts without gas from GIM6 and the RC decreases from ~2% to ~1%. When gas is injected from GIM6, for the low recycling case, the density is raised from ne ~$2\times n_{cut\text{-}off}$ (RC~4%) to n_e~$4\times n_{cut\text{-}off}$ (RC~1.5%) and for the high recycling case, the experimental density range is ~$6\times n_{cut\text{-}off}$ (RC~1%) to ne~$10\times n_{cut\text{-}off}$ (RC~0.5%) during ELMs. For the lower row, the figure does not show a simple relation between the density in front of the waveguides and the RC. Non-linear effects (i.e. coupling is power dependent) due to higher electrons/neutrals density could be responsible for this situation.

6. MODELLING OF THE SOL WITH POWER ABSORPTION FROM THE LH WAVE

An attempt to model the experimental modification of the density in the flux tubes passing in front of the LH antenna during power injection was performed. For that purpose, the two dimensional fluid code EDGE2D-NIMBUS [19] was modified in order to account for possible enhanced ionization in the SOL [20]. The JET poloidal limiters acting as sinks for the particles are also included in the model [21]. In this 2D model, the location of the gas injection is fully magnetically connected to

the LH antenna and the detailed effect of the exact arrangement of the different holes of GIM6 with respect of the antenna (i.e. loss of connection on the upper part) cannot be modeled. The enhanced ionization is obtained by assuming that a fraction of the LH power, called P_{abs}, is absorbed by the electrons in a layer extending in the radial direction from the launcher position to a radius located at a distance $D_{LW} \sim 0.02$m from the launcher. The particle and heat diffusion coefficients were set to $0.1m^2/s$ near the separatrix ($R-R_{sep} < 0.01$m) and $1m^2/s$ elsewhere in the SOL. The modeling was performed for pulse 66972 (figure 3a). From the computed electron density and temperature profiles, the j_{sat} signal is reconstructed in order to compare to the measurement. When $P_{abs}=0$, a steep j_{sat} profile is obtained through the entire SOL (figure 13). This profile is quite consistent with the experimental one, as shown on figure 3b. Calculations done for the case PLH=0.4 and 1.6MW, show good agreement with the experimental data assuming $P_{abs}=10$ or 50 respectively (in normalized units for power in the code). The ratio of these values is almost the same as for the experimentally used LH powers. This result indicates that the dissipated power in the edge is a constant fraction of the launched power. The code indicates that the j_{sat} increase results from both an increase in n_e and Te. It should be stressed that this fluid code just considers the heating of thermal electrons; the computed enhanced ionization rate of the neutrals does not take into account fast electrons resulting from interaction between the high parallel index part of the launched wave spectrum and the thermal electrons [22]. This part of the spectrum, which accounts for less than 5%, does not contribute significantly to the current drive.

According to modeling the electrons have an average energy of 200-300eV for this amount of LH power. However the low density of these fast electrons (<10% of the total electrons) could have a minor effect as the ionization rate is enhanced by no more than a factor 2.5 (for D2) when the electron energy increases from 20eV to 300eV (this energy also corresponds to the maximum value for the ionization cross-section [23]). We therefore expect these fast electrons to account for no more that ~25% in the increase of the ionization rate.

The effect of the diffusion coefficient was also tested by changing the diffusion coefficient D in the SOL ($0.03 < R-R_{sep} < 0.05$) from 0.7 to $1.3m^2/s$. This results in an increase of J_{sat} by less than 20% in the plateau region only if an additional source term ($P_{abs}=150$ in normalized code units) is included. When D is reduced from 1 to $0.3m^2/s$ in the region ($0.03<R-R_{sep}<0.05$m), j_{sat} is almost divided by 2 in this zone but the decrease of j_{sat} is weaker in the plateau zone. According to this model, the experimental jsat data indicate that the value of the diffusion coefficient lies in-between these two values (figure 14). With no additional power source dissipated in the SOL, no reasonable value of the diffusion coefficient can be found to explain the experimentally observed very flat j_{sat} profile in the far SOL. This conclusion is opposite to the one from early experiments for which the change in the profile of transport coefficient seems to offer the only mechanism by which the edge density modification (increase of density by a factor ~2) can be reproduced by EDGE2D [23].

7. HOT SPOTS ON COMPONENTS CONNECTED TO THE LH LAUNCHER

LH power absorption in the flux tubes passing in front of the antenna may lead to enhanced ionization of the gas but can also produce in the SOL a fast electron tail in the velocity distribution function in a way very similar to the acceleration of fast electrons in the plasma core by Landau damping. For the low temperature electrons of the SOL, the very high components of the parallel refraction index of the wave are damped and electrons can be accelerated up to a few keV. This leads to fluxes which can be of the order of several MW/m2 on plasma facing components connected to the flux tubes [22, 25, 26] where these fast electrons are generated.

On JET, heat power deposition on the upper part of the divertor has been observed with a CCD camera during LHCD experiments [15]. Field line tracing and hot spot topology give evidence for the nature of the particles carrying this heat flux. The infra-red camera recently installed on JET now also allows to quantify the heat flux. This was performed for two shots using surface temperature measurements of the left-hand side limiter (MTL3) of the new ITER-like ICRH antenna (ILA), located toroidally ~45° in the ion drift direction from the LH antenna (L//~3m). From field line tracing it can be concluded that the hot spots on MTL3 are connected to the lower part of the LH antenna. More precisely, the analyzed tiles labelled 8 and 9 are connected to row 5 and 4 respectively'. Depending on the actual radial position of the LH antenna (for which an uncertainty of 25mm toward the plasma is assumed), the radial extension of the field lines passing in front of the antenna and connected to the side limiter (d_0) can vary between d_0=7.5 and d_0=15mm. The two discharges have various phases in H and L mode with 0.5MW < P_{LH} < 3MW. The temperature was modeled with the 2D version of the thermo-hydraulic code CAST3M. For each phase the parallel heat flux $F_{//0}$ was adjusted to fit the experimental data. The experimental and computed temperature is plotted as a function of time in figure 15 for the case where d_0=7.5mm. Two power deposition profiles were assumed: constant parallel flux on the limiter tile (peaking factor PF=1) and linear increase of the flux with radial distance from the antenna (peaking factor PF=1.5). The good agreement between experiment and modeling of the temperature in particular in the decay phases with no LH power leaves an uncertainty on the peaking factor and indicates that effects due to thin carbon layers often observed on plasma facing components are in this case weak and probably For the two shots, the plot of $F_{//0}$ as a function of the LH power (figure 16) has two main features: for the same LH power, the heat flux is lower in H mode than in L mode and for the same confinement regime, the heat flux scales roughly like the square of the LH power. For the power dependence, a similar result was found on Tore Supra [26]. These two features results from the same cause, the electron density increases near the grill when the plasma transits from the H mode to the L mode for the first one and when the LH power increases for the second one. When the radial penetration of the fast electron beam is reduced from d_0=15mm to d_0=7.5mm on the side limiter tile, the heat flux $F_{//0}$ is increased by a factor ~1.8. The effect of peaking factor is moderate as the mean $F_{//0}$ is reduced by only ~15% (and therefore the peak value of F//0 is increased by ~30%) when the peaking factor increases from F=1 to F=1.5. By optimizing the density (i.e. reducing the gas injection), it is expected the flux not

to exceed 5MW/m^2 with P_{LH}~5MW in H mode.

During the H-mode phase, type-I ELMs (f~60Hz for the pulse of figure 15) have no measurable effect on the surface temperature although the IR frame frequency (~100Hz) is significantly larger. The expected effect of the ELMs on the surface temperature was investigated by assuming that the heat flux was varying with time as a linear function of the ELM amplitude. This rough approximation is reasonable when one considers that the heat flux, for a given LH power, is proportional to the edge density. The average flux was adjusted to model the experimental temperature and the largest variation of heat flux was considered, i.e. no flux between ELMs. For the selected time window, this leads to a peak flux during the largest ELMs F//~12MW/m^2 for a case with $F_{//0}$=2.6MW/m^2. From this model, it results a temperature modulation of only 2-3°C which is consistent with the measurements.

DISCUSSION AND CONCLUSIONS

RCP measurements during high LH power coupling performed on H mode plasmas with a large gap between the LCFS and the antenna (0.12-0.15m) indicate a strong modification in the far SOL ($R-R_{sep}$>0.05m) when the probe is magnetically connected or almost connected to the array of LH waveguides (figure 1). For sufficiently large LH powers (PLH>1MW) this leads to a plateau in the density profile extending typically 0.05m in front of the JET poloidal limiters. By combining the beneficial effect of LH power and gas injection from a pipe connected to the antenna, the particle flux (j_{sat}) at the wall (i.e. front face of the poloidal limiters) can be increased by at least a factor 5. The LH coupling measurements are found to be consistent with these probe measurements and, practically, a threshold of $j_{sat}=10^6$A/m^2 measured at the wall (i.e. 0.02m in front of the LH launcher) is found to ensure a good coupling of the wave. The strong transition from weak to good coupling suggests that the very flat density profile could extend in the 'private' plasma of the LH antenna, behind the poloidal limiters. This would lead in some cases to a density, at the plasma-antenna interface, exceeding by far the optimal density ne~$3\times n_{cut-off}=5\times10^{17}m^{-3}$. This high density is also supported by the weak increase of the RC which is consistent with a computed density $n_e>1\times10^{18}m^{-3}$. However for these case of high density (and probably higher electron temperature), the local high particle recycling and/or higher neutral pressure may lead to non-linear effects for the coupling wave although this has never been clearly observed in the past experiments. All these results confirm that the optimal density has been exceeded in many cases and the gas injection has to be adjusted during the pulse when the LH power is varied (ramp-up phase) and/or recycling conditions are changing. Maintaining J_{sat} at the wall between 1 and 1.5×10^6A/m^2 seems to be an optimum. Under this condition, the extrapolation of the present results to higher powers (4-6MW) indicates that the required gas flow should be lower than 2×10^{21}el./s for the studied scenarios. This is a favourable situation as high gas injection may have a deleterious effect on plasma confinement and the gas rate for a 20MW antenna, as envisaged on ITER, is expected to be low with respect of the total gas rate. The local increase of the density with the LH power is further documented by analysis of

the hot spots resulting from the interaction of connected plasma facing components with electrons accelerated on the near-field of the antenna. With constant gas injection, the heat flux scales as the square of the LH power whereas the modelling predicts a linear effect of the power when only RF field effects are considered.

During the ELMs, the particle flux (and therefore the density) may increase at the wall by more than one order of magnitude, even with a gap of 0.10m between the wall and the LCFS. Although this parameter cannot be measured in the private plasma of the LH antenna, the relative increase of density should be of the same order. The transient decrease or increase of the RCs confirms that high density can be reached with large ELMs, 0.15m behind the LCFS. Different behaviours for the lower part and the upper part of the antenna suggest that the gas injection could be more efficient in the lower part. With type I ELMs, no loss of power coupled to the plasma is observed up to RF power density of 22MW/m^2 (averaged on 1/6 of the full antenna) and the predicted resilience of RC to the SOL density is assessed for a multijunction LHCD antenna. Modelling of the heat flux due to electrons indicates that a modulation of this flux at the ELM frequency does not contribute significantly to the surface temperature of the component consistently with the IR images.

Simple 2D modelling of the interaction of the LH waves with the plasma of the SOL shows that such flat profiles can be obtained by assuming that a small fraction of the power is absorbed in a 2cm thick plasma layer facing the antenna. The computed linear scaling of the plateau density with LH power is also consistent with the measurements. Further modelling is needed to rule out completely or partially the effect of enhanced particle and heat diffusion in order to assess the beneficial effect of enhanced neutrals ionization by wave damping in the far SOL.

ACKNOWLEDGEMENT

This work, supported by the European Communities under the contract of Association between EURATOM and CEA, was carried out within the framework of the European Fusion Development Agreement. The views and opinions expressed herein do not necessarily reflect those of the European Commission. One of the authors (V.P.) was supported in part by the Czech Science Foundation Project GACR 202/07/0044

REFERENCES

[1]. Tuccillo A A et al ,2005 Plasma Phys. Control. Fusion **47** B363
[2]. Litaudon.X et al., Plasma Phys. Control. Fusion 48 (2006) A1–A34
[3]. Ide S et al Nucl. Fusion **40** (2000) 445
[4]. Kukushkin AS, Nucl. Fusion 47 (2007) 698–705
[5]. Leuterer F et al., Plasma Phys. Control. Fusion 33 (1991) 169
[6]. Ikeda Y et al., in Controlled Fusion and Plasma Physics (Proc. 15th Int. Conf., Sevilla, 1994), IAEA-CN-60/A3-1, IAEA, Vienna (1995) 415
[7]. Giruzzi G et al., High power coupling and investigation of fast electrons dynamics, Plasma

Physics and Controlled Nuclear Fusion Research , 1995 (Proc. of the 15th IAEA conference, Seville , 1994) ,Vol. 2 (IAEA, Vienna) 197[8]. T. Loarer, *et al*., this conference

[8]. Mailloux J et al., Long distance coupling of the lower hybrid waves on Tore Supra, Proc. of the 25th European conference on Cont. Fus. and Plasma Heating, Prague, European Physical Society, Vol.23, part I, (1998) 1394

[9]. Goniche M et al., Long distance coupling of lower hybrid waves in JET using gas feed, internal report JET-R(97)14, Abingdon, OXON,OX14 3EA, UK

[10]. Ekedahl A et al. Nucl. Fusion 45 (2005) 351-359

[11]. Pericoli Ridolfini V et al., Plasma Phys. Control. Fusion 46 (2004) 349-368

[12]. Lennholm M et al 1995 Proc. 16th IEEE/NPSS Symp. Fusion Engineering (Urbana-Champaign, Illinois, 1995) vol 1, p 754

[13]. Schild Ph. et al 1997 Proc. 17th IEEE/NPSS Symp. Fusion Engineering (San Diego, CA, 1997) vol 1, p 421

[14]. Erents K et al., Plasma Phys. Control. Fusion 46 (2004) 1757–1780

[15]. Rantamäki KM et al., Plasma Phys. Control. Fusion 47 No 7 (July 2005) 1101-1108 and ref. therein.

[16]. Litaudon X, Moreau D, Nuclear Fusion, 30 (1990) 471

[17]. Zohm H Plasma Phys. Control. Fusion 38 (1996) 105

[18]. Bécoulet M et al Plasma Phys. Control. Fusion 45 (2003)1-21

[19]. Simonini R et al., Contrib. Plasma Phys. 34 (1994) 2/3 368-373

[20]. Petržílka V et al., Proc, of the 33rd EPS Conference on Plasma Phys., Rome, 19-23 June 2006 ECA Vol.30I, P-1.067 (2006))

[21]. Petržílka V et al., Proc, of the 34th EPS Conference on Plasma Phys., Warsaw, 2-6 July 2007 ECA Vol.31F, P-4.100 (2007)

[22]. Fuchs V et al., Phys. Plasmas 3, 4023 (1996)

[23]. Janev RK et al, Elem.Proc.in Hydrogen-Helium Plasmas, Springer Verlag 1987)

[24]. Matthews GF et al.,.Plasma Phys. Contr. Fusion 44 (2002) 68

[25]. Mailloux J et al, J.Nuc.Materials, 241-243, p745 (1997)

[26]. Goniche M et al., Nuclear Fusion, 38 (1998) 919

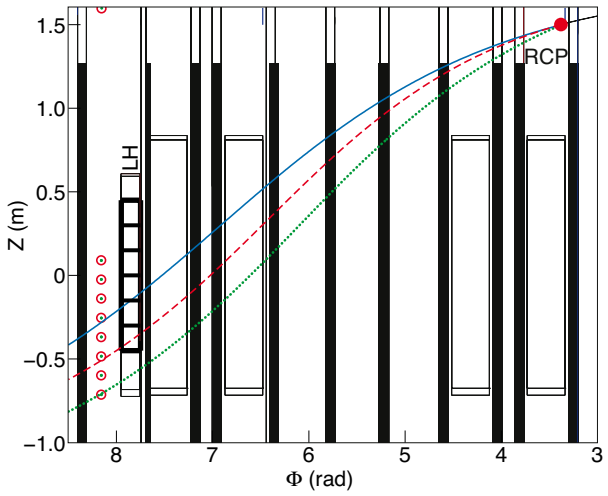

Figure 1: Field line tracing in the (Φ,Z) plane (R-R_{sep}=0) for three shots : #67882 (q_{95}=5.5, dotted line), #66972 (q_{95}=6.6, solid line) and #68948 (q_{95}=6.8, dashed line). PL are indicated by vertical black bars. The 8 holes of GIM6 are also indicated.

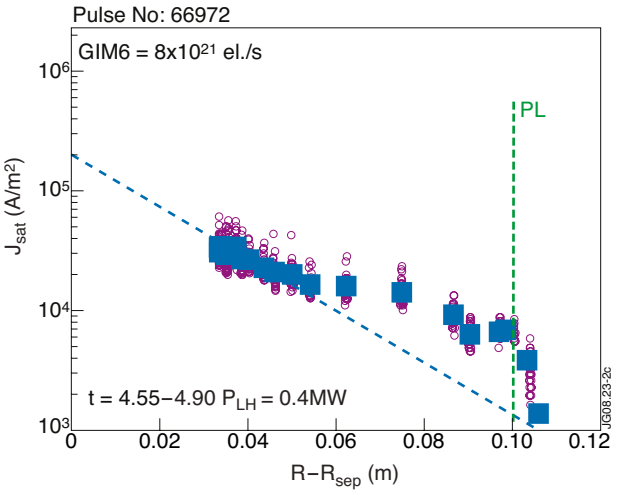

Figure 2: J_{sat} vs. R-R_{sep}. J_{sat} values averaged on radius slices (Δr<1mm) are indicated with the closed square symbols. The slope of the dashed line is for λ_J=0.02m. The position of the poloidal limiters (PL) is indicated by the vertical line. (B_t=3T, I_p=1.5MA, low triangularity plasma, n_l=7.4×$10_{18}m_{-2}$).

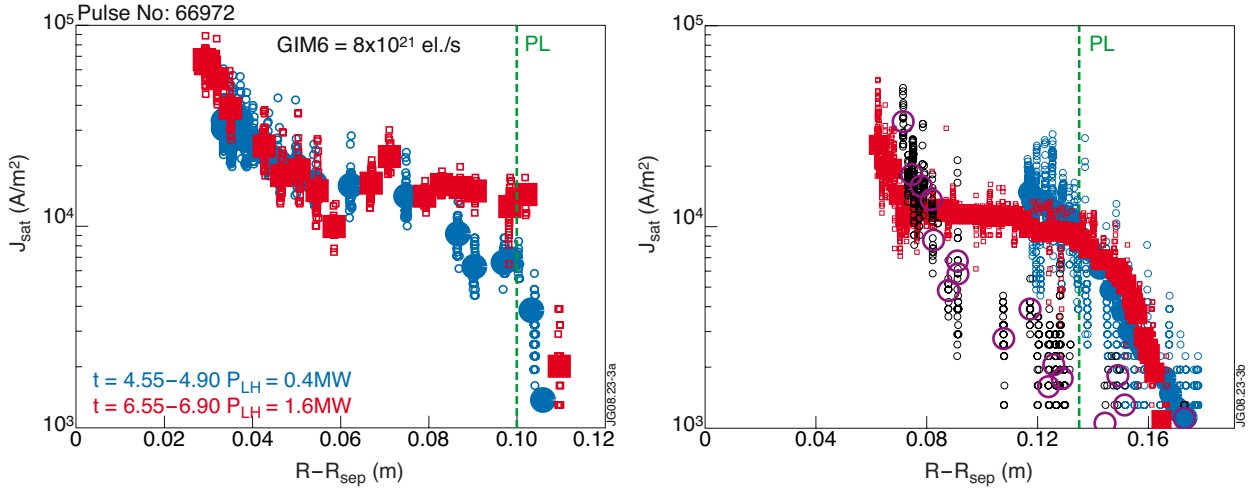

Figure 3: J_{sat} profile in the case of a) low triangularity plasma, D_{sa}=0.12m, F_{GIM6}=8×10^{21}el./s, P_{LH}=0.4MW(circles) and 1.6MW(squares). b) high triangularity plasmas, D_{sa}=0.15m, F_{GIM6}= 0, PLH=0.6MW (open circles), F_{GIM6}=4×10^{21}el./s, PLH=0 (closed circles) and F_{GIM6}=2×10^{21}el./s, PLH=3.2MW (closed squares). All data (small symbols) and time-averaged data (large symbols) are shown.

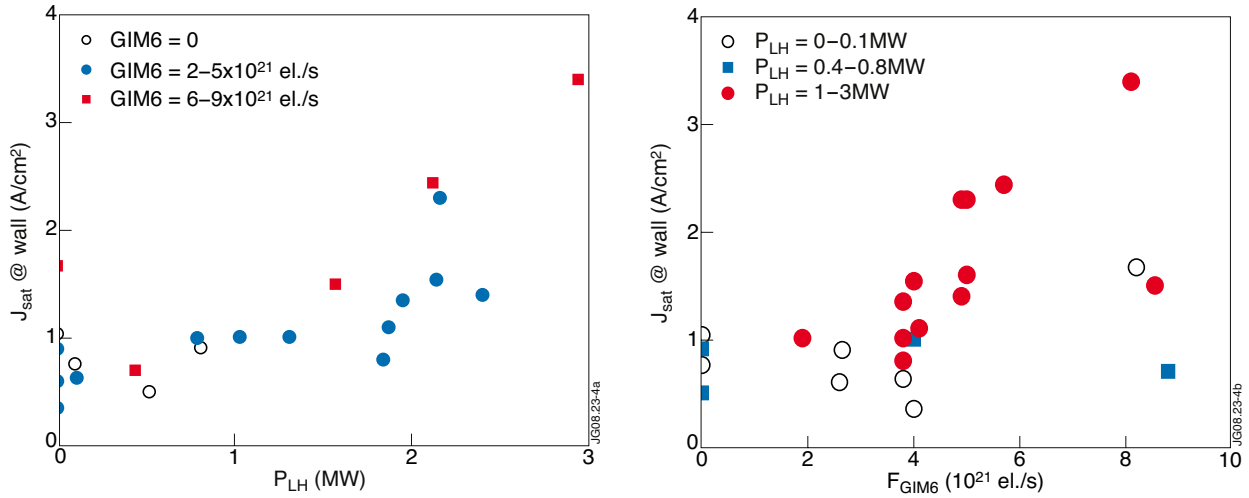

Figure 4: J_{sat} at the wall as a function of a) coupled LH power b) FGIM6 (Low δ plasmas, separatrix at 0.10m from the wall).

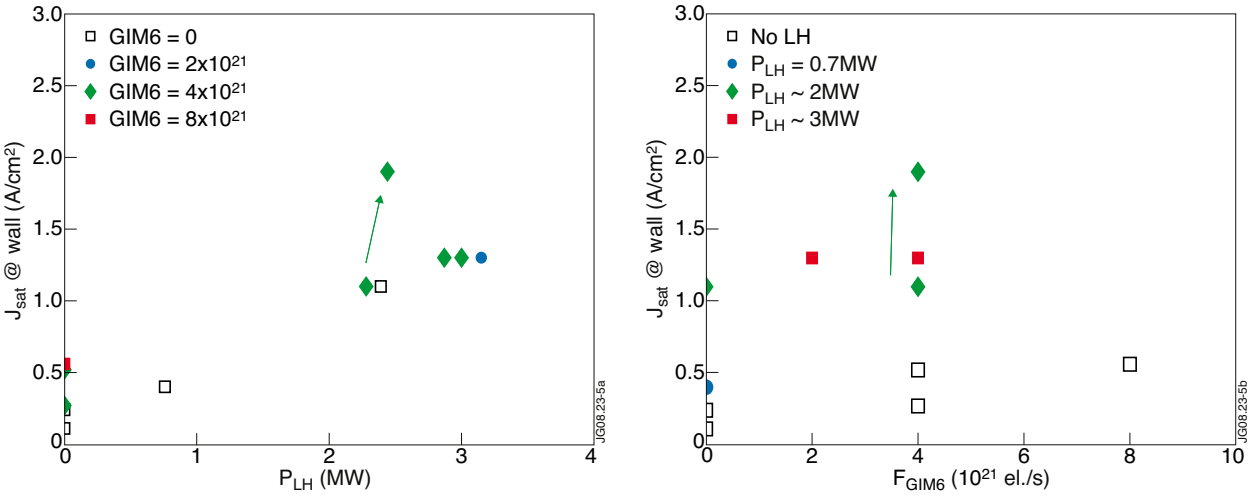

Figure 5: J_{sat} at the wall as a function of a) coupled LH power b) F_{GIM6} (High δ plasmas, separatrix at 0.13m from the wall). Effect of GIM9-10 injection is indicated by the arrows.

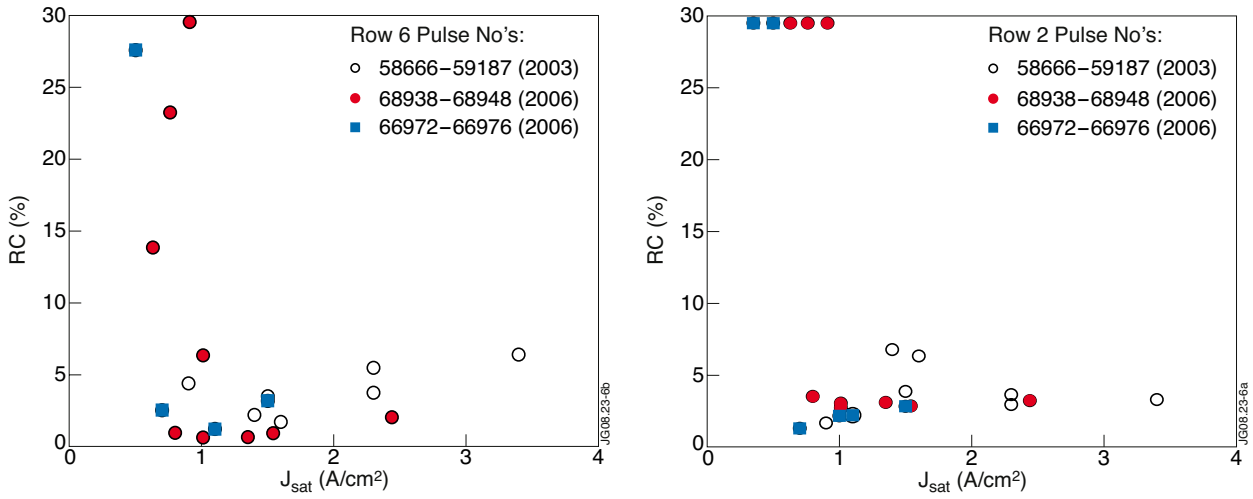

Figure 6: a) RC of upper row and b) bottom row (right) as a function of J_{sat}@wall (low δ case, separatrix at 0.10m from the wall).

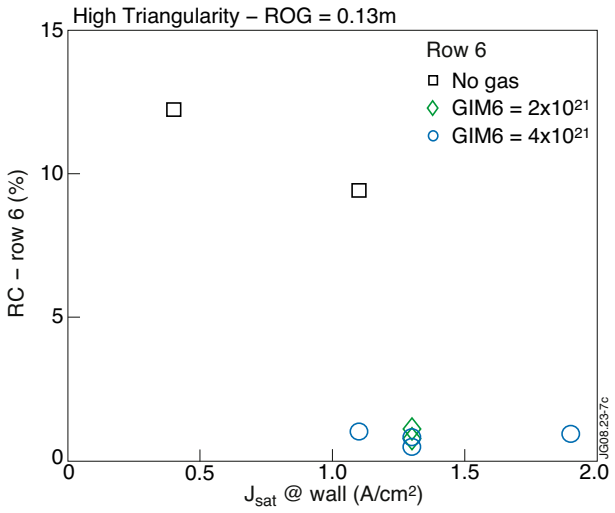

Figure 7: RC of row 6 as a function of J_{sat}@wall (high δ case, separatrix at 0.13m from the wall).

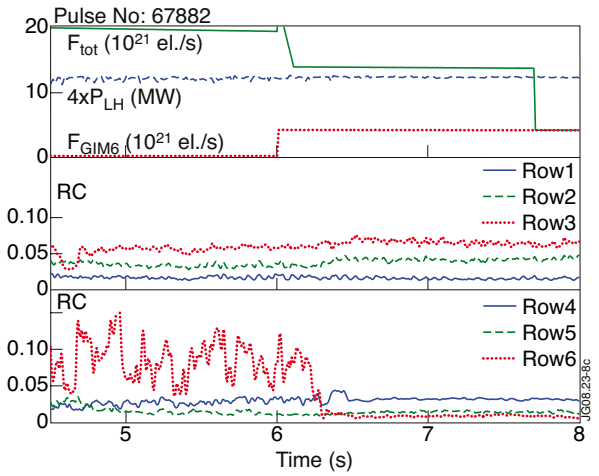

Figure 8: RC for the 6 rows of waveguides. LH power and gas injection are shown in the upper graph (High δ case, separatrix at 0.13m from the wall).

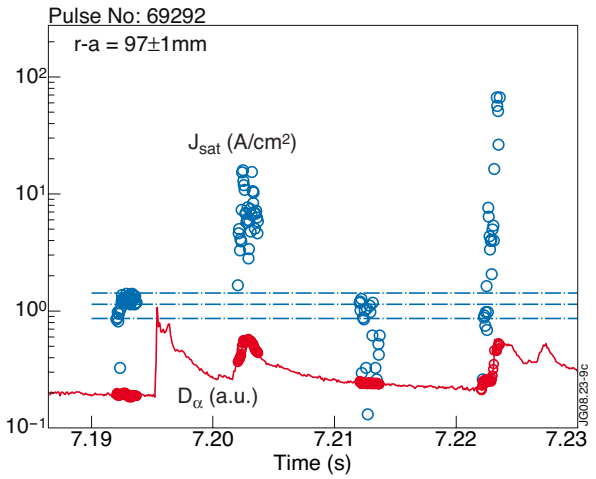

Figure 9: D_α (solid line) and J_{sat}@wall (open circles). D_α data during RCP measurements are indicated by bold symbols. The average Jsat between ELMs and $<J_{sat}>\pm$ one standard deviation are indicated by broken lines (high δ case, separatrix at 0.10 m from the wall, $F_{GIM6}=1.25\times10^{21}$el./s, F_{GIM9}-10=1.25×10^{21}el./s).

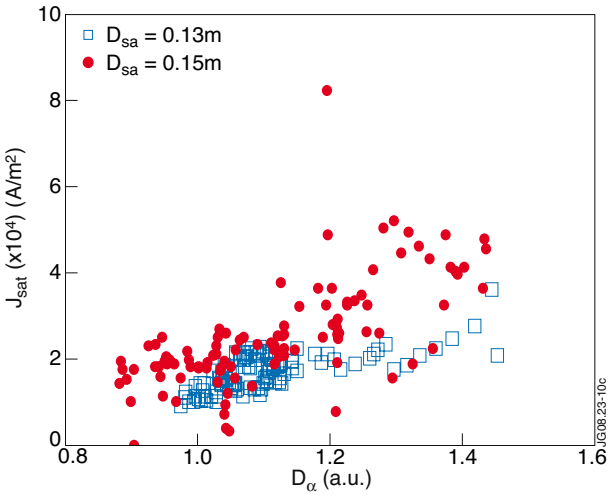

Figure 10: J_{sat} as a function of D_α for two locations: D_{sa} =0.13m (close circles) and D_{sa} =0.15m (opened squares). High δ case, separatrix at 0.13m from the wall, $F_{GIM6}=4\times10^{21}$el./s, $F_{GIM9\text{-}10}=10\times10^{21}$el./s

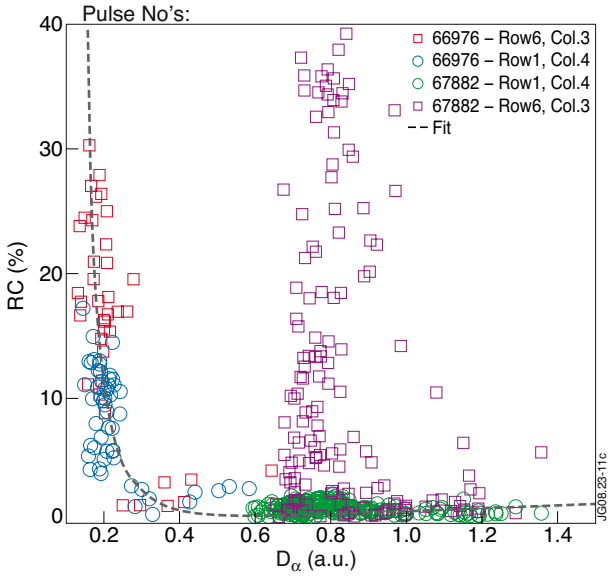

Figure 11: RC of a module of row 1 (circles) and row 6 (squares). Low δ case, D_{sa}=0.12m (D_α<0.6) and high δ case, D_{sa}=0.15m (D_α>0.6), F_{GIM6}=0.

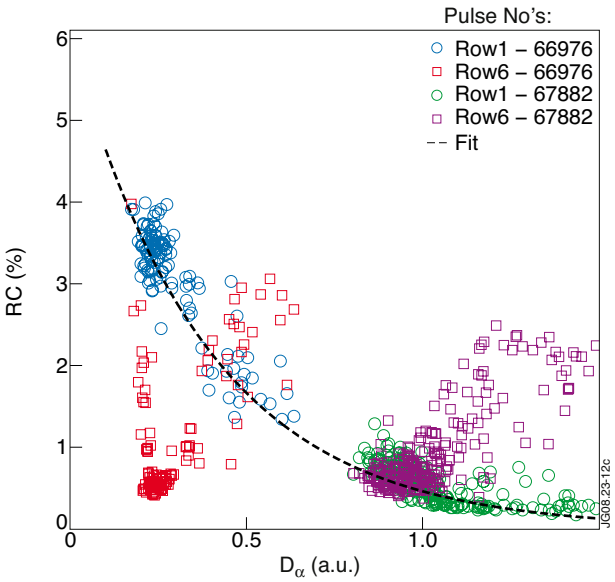

Figure 12: Same as figure 11 with $F_{GIM6}=4\times10_{21}$el./s. The RC is here averaged on four modules of the same row.

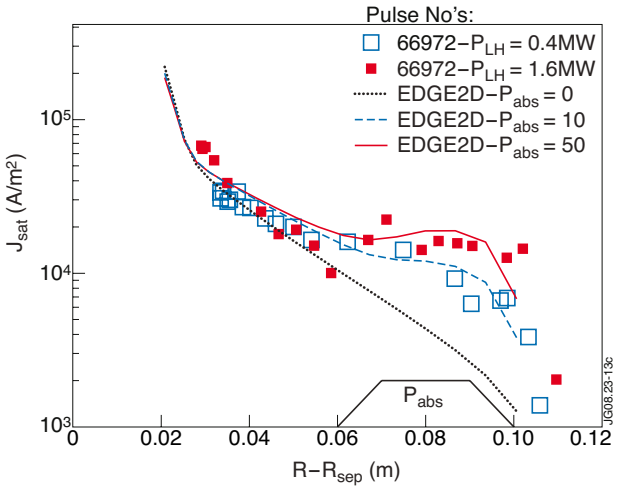

Figure 13: . Modelling of J_{sat} (pulse 66972) with P_{abs}=0 (dotted line) and P_{abs}=10 (dashed line) and P_{abs}=50 (solid line). DLW=0.02m. Experimental data (after time-averaging) are shown for P_{LH}=0.4MW (□) and P_{LH}=1.6 MW (■). Values for P_{abs} in normalized units as used in the code.

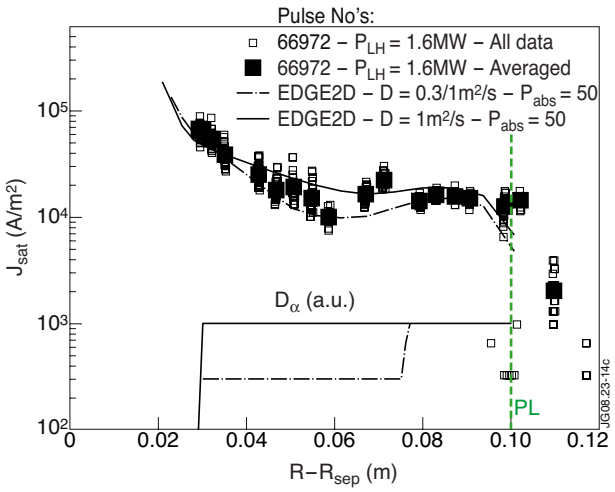

Figure 14: Modelling of J_{sat} (pulse 66972) with two values of the diffusion coefficient D=0.3m^2/s and 1m^2/s in the region defined by 0.03m<R-R_{sep}<0.05m (D= 1m^2/s for R-R_{sep}>0.055m).

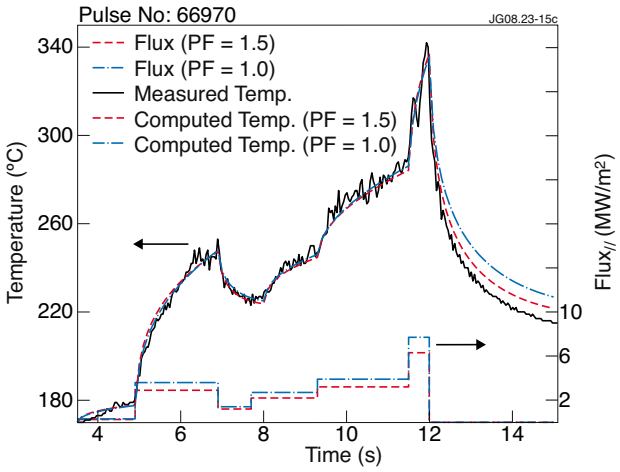

Figure 15: Time evolution of the temperature of tile 8 of the ILA side limiter (MTL3): measured (solid line) and calculated with two peaking factors for the power deposition, PF=1 (dot-dashed line) and PF=1.5 (dashed line). The corresponding parallel heat flux for these two computations are also shown. Pulse 66970, d_0=7.5mm. H mode for t < 7.8s, L mode later.

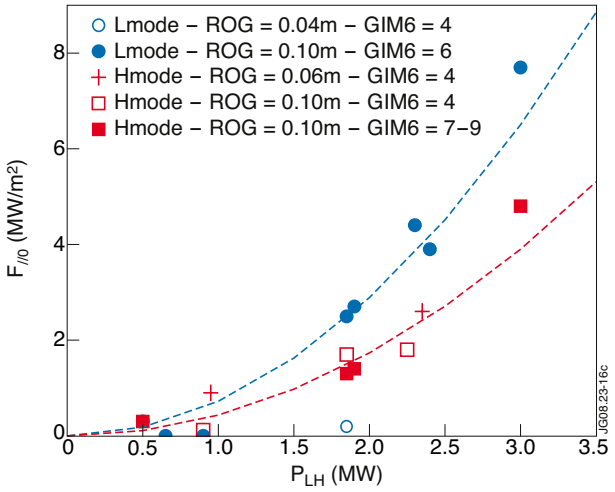

Figure 16: . F//0 vs. LH power for L mode (o) and H mode (+ and □) plasmas, d_0=15mm (pulses 66970 and 68938). Distance between LCFS and the PL (ROG) is varying between 0.05 and 0.10m. The highest heat flux from tile 8 or 9. Dashed lines are parabolic fits.